Journal of Molecular Structure 1312 (2024) 138412

Contents lists available at ScienceDirect

Journal of Molecular Structure

journal homepage: www.elsevier.com/locate/molstr

4-hydroxyquinolin-2(1*H*)-one isolated in cryogenic argon and xenon matrices: Tautomers and photochemistry

A. Secrieru [a,b], S. Lopes [c,*], T. Nikitin [c], Maria L.S. Cristiano [a], R. Fausto [c,d]

[a] CCMAR and Department of Chemistry and Pharmacy, FCT, Campus de Gambelas, University of Algarve, Faro 8005-039, Portugal
[b] Department of Chemistry, University of Liverpool, Liverpool L69 7ZD, UK
[c] CQC-IMS, Department of Chemistry, University of Coimbra, Coimbra 3004-535, Portugal
[d] Faculty of Sciences and Letters, Department of Physics, Istanbul Kultur University, Ataköy Campus, Bakirköy, Istanbul 34156, Turkey

ARTICLE INFO

Keywords:
4-hydroxyquinolin-2(1*H*)-one
Tautomers
Matrix isolation
IR spectra
Photochemistry

ABSTRACT

4-Hydroxyquinolin-2(1*H*)-one (4HQ2O) was synthesized, isolated in cryogenic matrices (argon and xenon), and studied by infrared spectroscopy. Quantum chemical calculations carried out at the DFT(B3LYP)/6–311++*G* (3df,3pd) level of theory were used to determine the conformational and tautomeric properties of the molecule. Two tautomeric forms were identified in the as-deposited matrices with the help of the theoretical data. To investigate the photochemistry of the compound, *in situ* broadband ultraviolet ($\lambda > 283$ nm) irradiation of the as-deposited argon matrix was performed. This irradiation led to the generation of an additional tautomer, together with the products of fragmentation of the heterocyclic ring of the molecule, specifically isocyanic acid and carbon monoxide. Photoproducts such as 1,3-dihydro-2*H*-indol-2-one and cyclohepta-1,2,4,6-tetraene were also observed in the photolyzed argon matrix. A comprehensive assignment of the infrared spectra of all the species observed experimentally is presented.

1. Introduction

Quinolines and their derivatives exhibit extensive biological activity [1–4]. Quinolinones, both natural and synthetic, in particular, have garnered significant attention due to their wide-ranging use in medicinal chemistry, serving diverse roles as antibacterial [5,6], antimicrobial [5,7], antitumor [6,8], anticancer [4,9], antimalarial [4], antifungal [4], as well as molluscicidal, and larvicidal agents [10]. Following the first synthesis of quinolone, nalidixic acid, many biologically active compounds within this general family have been described [11].

Quinolinones are composed of a benzene ring fused to a pyridine ring, creating a two-ring system. In 4-hydroxy-2(1*H*)-quinolones, a hydroxyl (-OH) group is attached to the pyridine ring at position 4. The remarkable chemical reactivity of 4-hydroxy-2(1*H*)-quinolinones places these compounds as highly sought-after building blocks in synthetic organic chemistry. Their derivatives are valuable not only for their various pharmaceutical applications [12–16] but also as crucial intermediates in the production of dyestuffs [17] and herbicides [12]. Certain 4-hydroxy-2(1*H*)-quinolinones play essential roles in nature [18,19], with 3-substituted-4-hydroxyquinolin-2(1*H*)-ones, in particular, identified as selective non-competitive agonists of *N*-methyl-D-aspartate (NMDA) receptors [20,21] and antagonists of α-amino-3-hydroxy-5-methyl-4-isoxazolepropionic acid (AMPA)-type glutamate receptors, in neurons [22].

Herein, we present an investigation of the structure (in particular, conformational and tautomeric properties) and photochemistry of the parent compound, 4-hydroxyquinolin-2(1*H*)-one (4HQ2O), isolated in low-temperature argon and xenon matrices, employing infrared (IR) spectroscopy. The interpretation of the experimental data was substantiated by theoretical calculations at the DFT(B3LYP)/6–311++*G* (3df,3pd) level of theory. Two tautomeric forms of the compound were identified in the as-deposited matrices, allowing for their detailed vibrational characterization. In addition, the effect of *in situ* broadband irradiation of the matrix-isolated (in argon) compound with UV light ($\lambda > 283$ nm) was explored. Irradiation was found to generate a third tautomeric form and cause fragmentation of the heterocyclic ring, with production of carbon monoxide and isocyanic acid, concomitantly with 1,3-dihydro-2*H*-indol-2-one and cyclohepta-1,2,4,6-tetraene. Overall, this investigation contributes to expanding the existing knowledge regarding the structure, tautomerism, and photochemistry of 4-hydroxyquinolin-2(1*H*)-ones.

* Corresponding author.
E-mail address: susylopes@qui.uc.pt (S. Lopes).

https://doi.org/10.1016/j.molstruc.2024.138412
Received 19 January 2024; Received in revised form 12 April 2024; Accepted 18 April 2024
Available online 25 April 2024

2. Computational details and results

2.1. Computational details

Quantum chemical calculations were performed with the Gaussian 16 software package (Rev. B.01) [23] at the DFT(B3LYP) [24–26] level of theory, using the 6–311++*G*(3df,3pd) basis set [27–29]. Relaxed one-dimensional (1-D) potential energy scans were undertaken to locate the minima and transition state structures of 4HQ2O and its tautomeric forms. The geometries were optimized using the TIGHT convergence criteria established in the software. Transition state structures for conformational interconversion were located using the synchronous transit-guided quasi-Newton (STQN) method [30]. The nature of all described stationary points on the studied potential energy surface (PES) was characterized through the analysis of the corresponding Hessian matrices.

The harmonic vibrational wavenumbers and infrared intensities of the relevant species were also calculated at the DFT(B3LYP)/6–311++*G* (3df,3pd) level and are provided in the Supplementary Information (Tables S1–S3). Wavenumbers were scaled by two factors, 0.954 for values above 3000 cm^{-1} and 0.978 for those below, primarily compensating for the effects of basis set limitations, the neglected electron correlation, and anharmonicity. The resulting (scaled) wavenumbers, along with the calculated intensities, were employed to simulate the spectra depicted in the figures. In these simulations, the absorptions were convoluted using a Lorentzian function with a full-width at half-maximum (FWHM) of 2 cm^{-1}. The vibrational analysis was supported by the animation of the vibrations of all calculated species, provided by the Chemcraft software [31].

The ultraviolet (UV) absorption spectrum of 4HQ2O was also calculated within the framework of the time-dependent DFT (TD-DFT) theory, employing the same functional and basis set utilized for the structural and vibrational analyses [32,33].

2.2. Computational results

2.2.1. Geometries and energies of 4HQ2O and its tautomeric forms and barriers for internal rotation

The molecular structure of 4HQ2O has been previously investigated using various experimental techniques, including UV [34], IR [34,35], and nuclear magnetic resonance (NMR) spectroscopies [34]. The compound has five tautomeric forms related by prototropism involving the hydroxy/oxo and amino/imino fragments of the molecule; however, only three tautomeric species have been considered in prior investigations [36–38]. Fig. 1 illustrates these tautomeric forms along with their possible conformers. Table 1 provides the relative energies of these species.

In 4HQ2O (an amino-hydroxy-oxo form), there is only one conformationally relevant degree of freedom, namely, the internal rotation of the hydroxyl group around the C—O bond. The calculations conducted

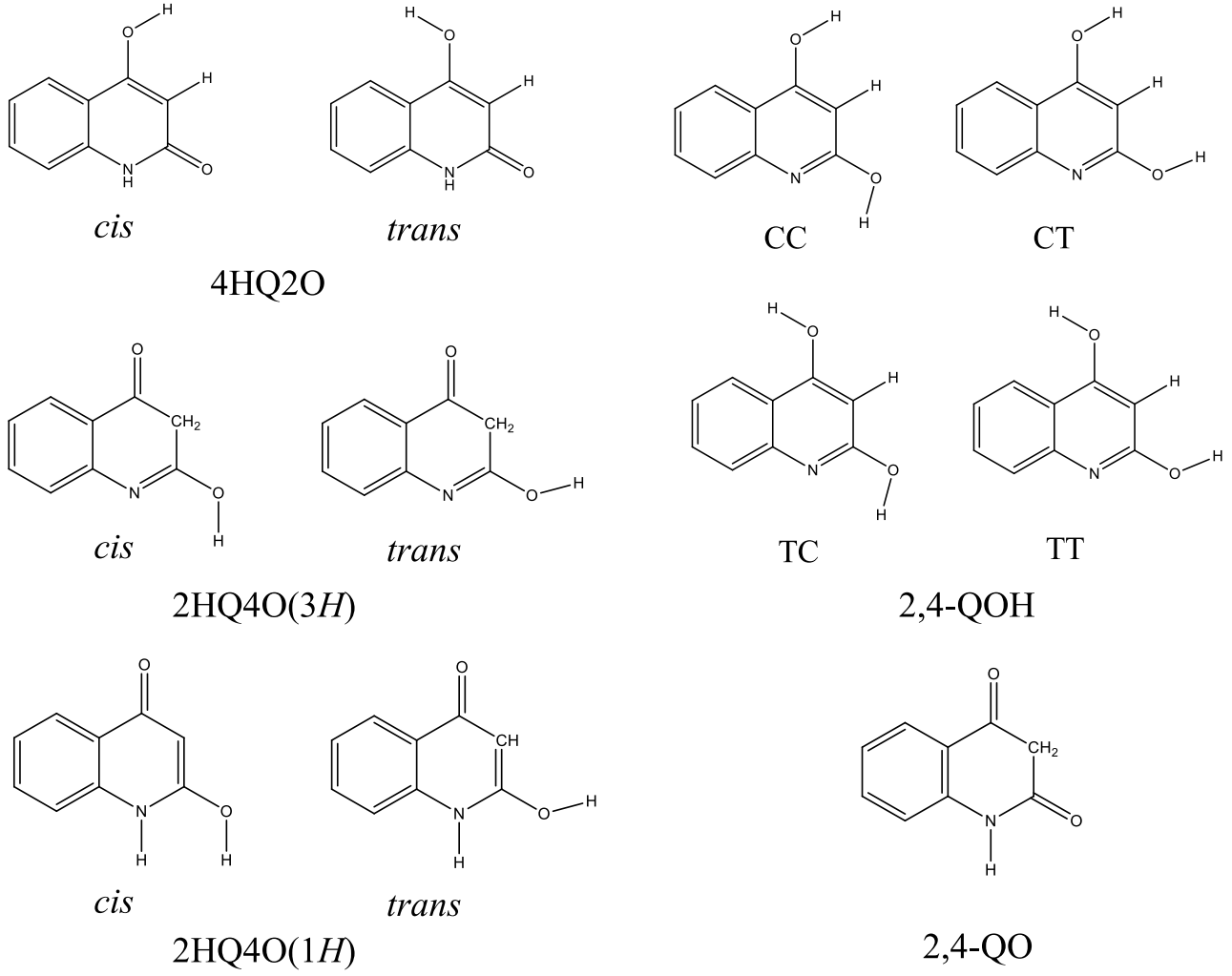

Fig. 1. Schematic structures of the 4HQ2O and its tautomeric forms and the corresponding conformers. The optimized structures obtained at the DFT(B3LYP)/6–311++*G*(3df,3pd) level, with atom numbering, are provided in Fig. S1.

Table 1
Electronic relative energies without (ΔE) and with (ΔE(0)) zero-point correction) and standard free Gibbs energies at 298.15 K (ΔG°) calculated at the DFT (B3LYP)/6–311++*G*(3df,3pd) level of theory for 4HQ2O and its tautomeric forms, and their corresponding conformers[a].

Form	ΔE	ΔE(0)	ΔG°
4HQ2O *cis*	0.0	0.0	0.0
trans	9.4	8.4	7.7
2,4-QO	7.5	4.8	1.9
2,4-QOH CC	20.9	20.1	20.6
CT	45.6	43.6	43.7
TC	25.3	23.8	23.9
TT	46.9	44.5	44.3
2HQ4O(3*H*) *cis*	51.3	47.8	45.3
trans	75.2	70.9	68.0
2HQ4O(1*H*) *cis*	53.4	50.6	49.5
trans	33.1	31.7	31.3

[a] Energies in kJ mol^{-1}. See Fig. 1 for schematic representation of the forms.

at the DFT(B3LYP)/6–311++*G*(3df,3pd) level of theory have unveiled the existence of two planar (C_s symmetry) conformers of the compound (refer to Fig. 1), which correspond to the *cis* and *trans* orientations of the OH group as defined by the C(3)=C(4)−*O*−*H* dihedral angle (0° and 180°, respectively). The *trans* conformer exhibits a higher energy compared to the *cis* form, with a measured difference of 9.4 kJ mol^{-1} (8.4 kJ mol^{-1} when including zero-point correction). This increased energy primarily stems from the stronger repulsive (O)H···H interaction in the *trans* conformer due to the closer proximity of the positively charged hydroxylic hydrogen and the ring hydrogen at position 5 (d(O)H···$H_{(C5)}$ = 1.882 Å). In contrast, the *cis* form features a lesser repulsion between the hydroxyl hydrogen and the ring hydrogen atom at position 3 (d(O)H···$H_{(C3)}$ = 2.312 Å). The calculated potential energy profile for internal rotation around the C–O bond, which interconverts the two conformers, is presented in Fig. S2. The energy barrier separating the two conformers is 24.1 kJ mol^{-1} in the *cis*→*trans* direction and 14.7 kJ mol^{-1} in the reverse direction (21.2 and 12.8 kJ mol^{-1}, respectively, including the zero-point correction).

Among all the tautomers of the studied compound, 2,4-QO (see Fig. 1) has the lowest energy, being 7.5 kJ mol^{-1} higher in energy than *cis*-4HQ2O (4.8 kJ mol^{-1} after inclusion of the zero-point correction). This tautomer, 2,4-QO, can be formed from *cis*-4HQ2O by migration of the hydroxylic hydrogen atom to the carbon at position 3 of the heterocyclic ring of the molecule, resulting in an amino-dioxo structure. It exhibits only one conformer (with two symmetrically-equivalent forms) that shows a geometry with the molecular skeleton slightly deviating from planarity, where the N–C(2)–C(3)–C(4) dihedral angle is ±16.6°. The remaining amino tautomer, 2-hydroxyquinolin-4(1*H*)-one (2HQ4O(1*H*)), like 4HQ2O, is an amino-hydroxy-oxo form. However, in this case, the hydroxylic group is situated at position 2 of the heterocyclic ring, while the carbonyl group is at position 4 (see Fig. 1). This tautomer features two conformers distinguished by the orientation of the hydroxylic group. The *trans* form (with an N–C–O–H dihedral of 180°) is the most stable one, being 33.1 kJ mol^{-1} higher in energy than *cis*-4HQ2O (31.7 kJ mol^{-1}, after consideration of the zero-point correction). Conversely, the (nearly) *cis* conformer (N–C–O–H dihedral equal to ±31.9°) is less stable, with a relative energy of 53.4 kJ mol^{-1}, *i.e.*, 20.3 kJ mol^{-1} higher than that of *trans*-2HQ4O(1*H*). When the zero-point correction is included, these energy differences are 50.6 and 18.9 kJ mol^{-1}, respectively. In the *trans*-2HQ4O(1*H*) form, a stabilizing interaction occurs between the nearly anti-parallel C–O and N–H bond-dipoles. This interaction is the primary factor contributing to the lower energy of this conformer relative to that of its *cis* counterpart, where a repulsive (O)H···H(N) interaction is present. The potential energy profile for interconversion between the two 2HQ4O(1*H*) conformers (and between the two equivalent-by-symmetry non-planar nearly *cis* structures) is presented in Fig. S3. The *trans*→*cis* energy barrier amounts to 22.3 kJ mol^{-1} (2.0 kJ mol^{-1} in the opposite direction), while that separating the two symmetry-equivalent non-planar *cis* forms is as low as 0.9 kJ mol^{-1}, staying only 0.3 kJ mol^{-1} above the zero-point level of the two *cis* minima.

In addition, there are two imino tautomers, 2-hydroxyquinolin-4(3*H*)-one (2HQ4O(3*H*)) and quinoline-2,4-diol (or 2,4-quinolinediol) (2,4-QOH), the first being an imino-hydroxy-oxo form and the latter an imino-diol form (Fig. 1). 2HQ4O(3H) has two high-energy conformers, which differ in the orientation of the hydroxylic group. The *cis* conformer has an energy higher than *cis*-4HQ2O by 51.3 kJ mol^{-1}, while the *trans* conformer exceeds it by 75.2 kJ mol^{-1} (the corresponding zero-point corrected values are 47.8 and 70.9 kJ mol^{-1}). The relative energies of the two conformers of 2HQ4O(3*H*) (23.9 kJ mol^{-1}; 23.1 kJ mol^{-1} after consideration of the zero-point correction) can be explained in a manner akin to that of 2HQ4O(1*H*). In this instance, the more stable *cis*-2HQ4O(3*H*) conformer bears a weak stabilizing interaction between the nearly anti-parallel O–H and C=N bond-dipoles, while the *trans* form is destabilized by repulsive (O)H···H_2(C(3)) interactions, stemming from the distinct orientation of the hydroxylic group. Fig. S4 shows the potential energy profile for the interconversion between the two 2HQ4O(3*H*) conformers, the calculated *cis*→*trans* barrier being 46.7 kJ mol^{-1} (22.8 kJ mol^{-1} in the reverse direction). On the other hand, 2,4-QOH may exist in four different conformational states, herein designated as CC, CT, TC, and TT, where C and T refer to *cis* and *trans* arrangements of the hydroxylic groups, respectively. In this notation, the first letter is related to the conformation defined by the dihedral angle C(3)=C–O–H, whereas the second is related to that defined by the dihedral angle N=C–O–H. The two conformers of 2,4-QOH featuring a *cis* arrangement of the N=C–O–H fragment (CC and TC) are significantly more stable than the *trans* counterparts (CT and TT). The CC and TC forms have energies higher than that of *cis*-4HQ2O by 20.9 and 25.3 kJ mol^{-1}, respectively (zero-point corrected values: 20.1 and 23.8 kJ mol^{-1}), while the *trans* N=C–O–H 2,4-QOH conformers are high-energy species, with relative energies of 45.6 (CT) and 46.9 (TT) kJ mol^{-1} above *cis*-4HQ2O. If the zero-point corrections are considered, the energies of the CT and TT 2,4-QOH conformers become 43.6 and 44.5 kJ mol^{-1}, respectively, above that of *cis*-4HQ2O (*i.e., ca.* 20 kJ mol^{-1} above those of the corresponding *cis*-2,4-QOH counterparts). The rationale for the relative energies of the conformers of 2,4-QOH mirrors that proposed for 2HQ4O(3*H*) and 2HQ4O(1*H*). The most stable conformers of 2,4-QOH are stabilized by a weak interaction between the nearly anti-parallel O–H and C=N bond-dipoles, whereas in the two higher-energy conformers, this interaction is replaced by a repulsive (O)H···H(C(3)) interaction. The calculated potential energy profiles for interconversion between the conformers of 2,4-QOH are shown in Fig. S5. All the energy barriers for interconversion between the different pairs of conformers of 2,4-QOH, taken in the direction corresponding to the conversion of the higher energy form into the lower energy form, are similar and fall within the 15.7–18.4 kJ mol^{-1} range. In the opposite direction, the energy barriers of conversion between the two *cis* N=C–O–H conformers (CC and TC) and between the two *trans* N=C–O–H conformers (CT and TT) are 22.0 and 19.7 kJ mol^{-1}, respectively, while those between the two *cis* C=C–O–H conformers (CC and CT) and between the two *trans* C=C–O–H conformers (TC and TT) are considerably higher, amounting to 40.4 and 40.0 kJ mol^{-1}, respectively.

Several bond lengths undergo significant changes owing to the tautomerization. As expected, the calculated NC(2) bond length varies from 1.39/1.40, 1.37/1.36, and 1.38 Å, in the amine tautomers (*cis/ trans* 4HQ2O, *cis/trans* 2HQ4O(1*H*), and 2,4-QO, respectively), to 1.27 and 1.30 Å in the imino forms (*cis* and *trans* 2HQ4O(3*H*) and all conformers of 2,4-QOH, respectively), clearly revealing the change from an essentially single bond into a predominantly double bond. The same applies to the C(2)C(3), C(3)C(4), and C(4)C(5) bonds, involving the carbons bearing the oxygen atoms (C(2) and C(4)), which are longer when they are formally single bonds, *e.g.* in 4HQ2O (*cis*: 1.45, –, 1.44 Å, *trans*: 1.44, –, 1.45 Å, respectively), 2HQ4O(3*H*) (*cis*: 1.49, 1.52, 1.47 Å; *trans*: 1.50,

1.53, 1.47 Å), 2HQ4O(1*H*) (both conformers: –, 1.45, 1.49 Å), 2,4-QOH (CC: 1.41, –, 1.43 Å, TC: 1.42, –, 1.42 Å, CT: 1.41, –, 1.43 Å, TT: 1.42, –, 1.43 Å) and 2,4-QO (1.51, 1.52, 1.48 Å), than when they are formally double bonds, *i.e.*, C(3)C(4): 1.35 and 1.37 Å, in both the conformers of 4HQ2O and 2,4-QOH, respectively, and C(2)C(3): 1.35 and 1.36 Å, in *cis*- and *trans*-2HQ4O(1*H*).

The C(3)–C(2)–N bond angles also vary among the different tautomeric species, depending on whether the central carbon belongs to a C=O or COH group. These angles are smaller when the central carbon belongs to a C=O group, with values of approximately 114.4° in 4HQ2O and 116° in 2,4-QO. Conversely, the angles are larger when associated with a COH group, approximately 126° in 2HQ4O(3*H*), 123° in 2HQ4O (1*H*), and 125° in 2,4-QOH. Similarly, the C(3)–C(4)–C(5) bond angles follow the same general rule. The angle is smaller when C(4) belongs to a C=O group, ~116° in 2HQ4O(3*H*), ~115° in 2HQ4O(1*H*), and ~117° in 2,4-QO. On the contrary, it is larger when C(4) is connected to a hydroxyl group, with values 121.5° in 4HQ2O and ~120° in 2,4-QOH. It was pointed out before that for a formally sp^2 hybridized trigonal carbon atom, under the condition that no significant steric hindrance between the substituents occurs, the angle opposing a given bond reflects the amount of *p* character of that bond (in the case of the double bound, of its σ component), larger angles correlating with a larger *p* character of the bond [39,40]. In addition, the degree of *p* character of the bond is determined by the electronegativity of the atom connected to the central carbon atom, which is smaller for more electronegative atoms [39]. Being internal angles in a six-membered ring, both the C(3)–C(2)–N and C(3)–C(4)–C(5) angles obey the condition above. Therefore, it can be concluded that the ultimate reason for the smaller values of these angles when the central carbon atom belongs to a carbonyl group, compared to when it is connected to a hydroxylic moiety, is the smaller effective electronegativity of the carbonyl oxygen atom when compared with the hydroxyl one, which leads to a smaller *p* character of the bond and, consequently, to a smaller opposite angle. The smaller effective electronegativity of the carbonyl oxygen, compared to that of the hydroxylic oxygen, is clearly revealed by the smaller negative charges calculated for the first type of atom in the whole set of studied molecules (within the range –0.797 to –0.867 *e*) in comparison with those obtained for the second (–0.820 to –0.978 *e*).

3. Experimental details and results

3.1. Experimental details

3.1.1. Synthesis

Reagents for chemical synthesis were obtained from various suppliers, including Fluorochem, Apollo Scientific, Sigma Aldrich, Enamine, and Alfa Aesar, and were used without further purification. Proton (^{1}H) and carbon (^{13}C) NMR spectroscopy essays were conducted using a Bruker Avance III instrument operating at 400 MHz and 101 MHz, respectively. Deuterated dimethyl sulfoxide (DMSO-*d6*) was employed as the solvent for these analyses, and its residual peaks were used as internal references (at δ = 2.50 ppm and δ = 39.51 ppm for the ^{1}H and ^{13}C spectra, respectively). 4HQ2O was synthesized using a two-step method following the procedure by Chatterjee et al. [41] (Fig. 2). Initially, N1,N3-diphenylmalonamide (DPM) was prepared through a double nucleophilic substitution of diethyl malonate with aniline in a 1:2 ratio, using dimethylformamide as the catalyst. Subsequently, 4HQ2O was obtained through the cyclization of DPM *via* intramolecular Friedel-Crafts acylation catalyzed by polyphosphoric acid (PPA) at 150 °C. Melting point determination was performed using a Melting Point Apparatus SMP3, a Bibby Stuart Scientific instrument.

Synthesis of N1,N3-diphenylmalonamide, DPM:

A catalytic amount of dimethylformamide (DMF) was added to a stirred solution containing 9.8 mL of aniline (10 g, 108 mmol) and 8.25 mL of diethyl malonate (8.7 g, 54 mmol). The mixture was heated to 140 °C for 8 h, yielding a white crystalline precipitate, which was filtered and washed with ethanol to obtain the pure product without further purification. Yield: 5.17 g, 37%. Melting point: 230–231 °C. ^{1}H NMR (400 MHz, DMSO-*d6*) δ (ppm): 10.16 (s, 2H), 7.65 – 7.57 (m, 4H), 7.37 – 7.27 (m, 4H), 7.10 – 7.02 (m, 2H), 3.48 (s, 2H). ^{13}C NMR (101 MHz, DMSO-*d6*) δ (ppm): 165.41, 138.96, 128.76, 123.38, 119.06, 45.93. The characterization data for this compound are consistent with those reported in the literature [42].

Synthesis of 4-hydroxyquinoline-2(1*H*)-one, 4HQ2O:

Under agitation, DPM (4.8 g, 18.88 mmol) was gradually added to a solution of 84 % polyphosphoric acid (22.5 g) maintained at 150 °C. The reaction proceeded for 3 h, followed by quenching with ice water to generate a solid yellow precipitate. Subsequently, the precipitate was filtered and dissolved in 100 mL of 1 M NaOH. The insoluble residue was removed by filtration. Dropwise addition of concentrated HCl to the filtrate under agitation resulted in the precipitation of 4HQ2O, which was filtered, washed with distilled water, and dried under vacuum to obtain the desired pure product as a pale-yellow solid. Yield: 1.94 g, 64%. Melting point: 345–347 °C. ^{1}H NMR (400 MHz, DMSO-*d6*) δ (ppm): 11.22 (s, 1H), 7.78 (dd, *J* = 8.1, 1.5 Hz, 1H), 7.52 – 7.45 (m, 1H), 7.28 – 7.23 (m, 1H), 7.17 – 7.10 (m, 1H), 5.75 (s, 1H). ^{13}C NMR (101 MHz, DMSO-*d6*) δ (ppm): 163.65, 162.51, 139.22, 130.91, 122.71, 121.13, 115.19, 115.06, 98.27.

3.1.2. Infrared spectroscopy

The matrices were prepared by co-deposition of the sublimated compound and a large excess of the matrix host gas [Ar (N60) and Xe (N48) obtained from Air Liquide] onto a CsI substrate attached to the cold tip of the cryostat (APD Cryogenics closed-cycle helium refrigeration system with a DE-202A expander). The temperature of the substrate during the deposition of the matrices was maintained at 14 K in the case of Ar experiments and at 25 K for Xe experiments. The different deposition temperatures used in the experiments were chosen to guarantee optimal matrix optical properties in each case. In both cases, the spectra were acquired at 14 K. For deposition, the compound was placed in a specially designed homemade temperature-variable mini-oven attached to the cryostat through a needle valve. The temperature used to sublimate the compound (*ca.* 423 K) was monitored by a thermocouple placed inside the oven, while the valve nozzle was kept at room temperature (298 K). The temperature of the CsI substrate of the cryostat was measured directly at the sample holder using a silicon diode sensor connected to a digital temperature controller (LakeShore 335) with an accuracy of 0.1 K.

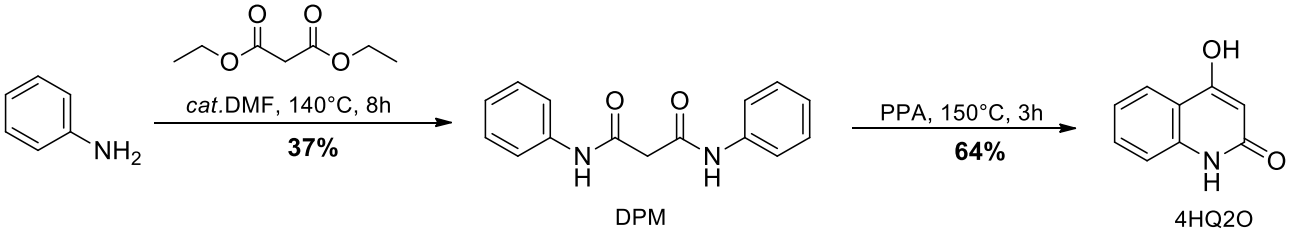

Fig. 2. Synthesis of 4-hydroxyquinoline-2(1*H*)-one (4HQ2O).

The IR spectra were obtained in the 4000−450 cm^{-1} mid-IR range using a Thermo Nicolet 6700 Fourier transform infrared spectrometer, equipped with an ETC EverGlo globar source, a deuterated triglycine sulfate (DTGS) detector, and a potassium bromide (KBr) beam splitter, with 0.5 cm^{-1} spectral resolution. To avoid interference from atmospheric H_2O and CO_2, a stream of dry CO_2-filtered air was continuously purging the optical path of the spectrometer.

Broadband UV irradiation of the matrices was carried out using a 200 W high-pressure Hg(Xe) lamp (Newport, Oriel Instruments) fitted with a water filter through the outer quartz window of the cryostat and using an additional long wave pass optical filter ($\lambda > 283$ nm).

3.2. Experimental results

3.2.1. Infrared spectra of matrix-isolated 4HQ2O

The infrared spectra of 4HQ2O isolated in argon and xenon matrices are presented in Fig. 3(a) and (b). As shown in the figure, the experimental spectra are well reproduced when the DFT(B3LYP)/6–311++*G* (3df,3pd) calculated spectra of *cis*-4HQ2O and 2,4-QO are considered together (Fig. 3(c)), demonstrating that both species are present in the as-deposited matrices. It is also worth mentioning the remarkable similarity between the profiles of the two experimental spectra. Most bands show site-splitting, indicating the existence of multiple trapping sites in both matrices, which is a common feature in matrix isolation IR spectroscopy. Tables 2 and 3 provide the proposed band assignments, which were facilitated by the good general agreement between the calculated and experimental data.

Considering the calculated relative Gibbs energies of the two conformers of 4HQ2O (7.7 kJ mol^{-1}; Table 1), the expected gas phase equilibrium populations of the most stable *cis* and higher energy *trans* forms are 89.9 % and 10.1 %, respectively, at 423 K (the temperature of sublimation of the compound) and 95.7 % and 4.3 % at room temperature (298 K), which was the temperature of the nozzle in the performed experiments. The latter temperature determines the equilibrium in the gas phase immediately prior to deposition of the vapor of the compound onto the cold optical substrate of the cryostat, meaning that without further considerations we could expect to experimentally observe both conformers. Moreover, the calculations indicated that the *trans*-4HQ2O → *cis*-4HQ2O isomerization energy barrier is 12.8 kJ mol^{-1} (after consideration of the zero-point correction), which is high enough to prevent the over-the-barrier *trans* → *cis* isomerization. Nevertheless, it falls within the range known to facilitate fast conformational relaxation of the hydroxyl group *via* quantum mechanical tunnelling. This mechanism was shown previously for many compounds bearing this group connected to an sp^2 hybridized carbon belonging to a ring under matrix-isolation conditions [43–45]. Consequently, it was not surprising that the obtained IR spectra of the prepared matrices of the studied material showed no compelling evidence of the presence of the higher-energy *trans*-4HQ2O conformer. On the other hand, the observation of the 2,4-QO tautomer in the as-deposited matrices was also not a surprise. Tautomerization upon sublimation, presumably taking place in the solid-gas interface, has been observed many times, in particular when the tautomeric forms involved have similar energies. A well-known example is the case of cytosine, where all its 4 lowest tautomeric forms (one of them exhibiting two conformers) were observed in argon matrices immediately after their preparation, with relative populations matching well their predicted gas phase equilibrium populations prior to deposition [46]. In the case of the presently studied chemical system, the Gibbs energy (at 298 K) of 2,4-QO was calculated to be only 1.9 kJ mol^{-1} higher than that of *cis*-4HQ2O (Table 1). Following the above trend, these two species appear to be present in the as-deposited matrices in a relative amount that should not differ significantly from those estimated for the equilibrium gas phase populations of the two forms at a temperature close to the sublimation temperature of the sample in the performed experiments. It is assumed here that this temperature is relevant in determining the tautomerization process at the solid-gas interface during sublimation, most probably in a process involving more than one participating molecule and an intermolecular H-transfer. It is important to note the fundamental difference when this is compared to the aforementioned conformational *cis*-4HQ2O / *trans*-4HQ2O

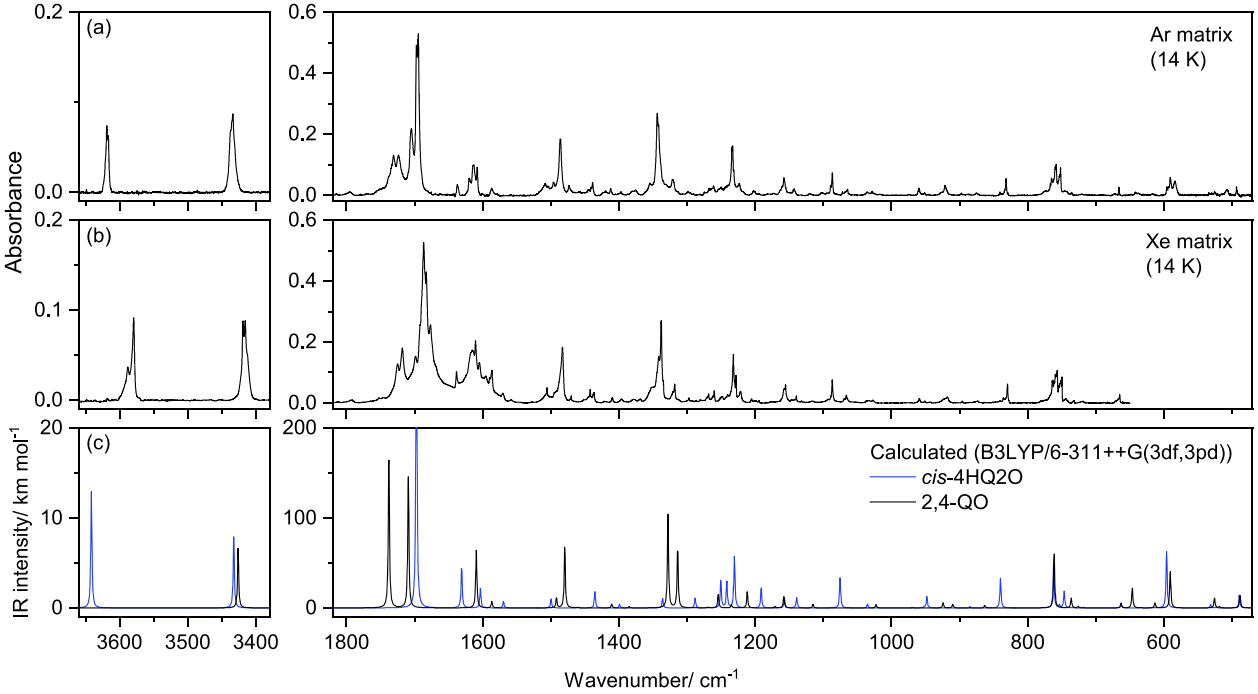

Fig. 3. Experimental IR spectra of the as-deposited argon (a) and xenon (b) matrices (14 K) of a sample of 4HQ2O, compared with the DFT(B3LYP)/6–311++*G* (3df,3pd) calculated IR spectra of *cis*-4HQ2O and 2,4-QO species (c). Bands due to minor traces of matrix-isolated water have been subtracted from the experimental spectra. The calculated harmonic wavenumbers were scaled by 0.978 and 0.954 for wavenumbers below and above 3000 cm^{-1}, respectively. The most intense band at 1697 cm^{-1} in panel c has been truncated for clarity.

Table 2
Experimental (matrix-isolation) and DFT(B3LYP)/6–311++*G*(3df,3pd) calculated infrared spectra of *cis*-4HQ2O and proposed vibrational assignments[a].

Approximate Description[b]	Experimental[c]		Calculated[d]	
	Argon matrix ν	Xenon matrix ν	ν	I^{IR}
ν(OH)	3619.0/3617.0	3588.0/3579.0	3641.5	77.8
ν(NH)	3437.5/3434.0	3419.0/3416.0	3432.6	44.9
ν(CH)	3092.0/3068.0/	3089.0/3068.0/	3065.1	4.2
	3059.0/3042.0	3059.0/3048.0/	3048.8	9.0
		3030.0	3046.5	2.4
			3036.9	8.1
			3023.7	2.5
ν(C=O)	1697.0/1695.0	1692.0/1687.0/	1697.2	927.1
		1683.0/1676.5		
ν(CC)	1637.0	1638.0	1630.8	119.6
	1613.0/1601.0	1610.5/1605.0	1603.3	57.8
	1579.0	1570.5/1558.0	1569.4	18.0
ν(CC), δ(CH)	1508.5/1504.5	1506.0/1503.0	1499.5	24.0
δ(CH)	1473.0	1470.0	1460.7	2.4
δ(COH), δ(CH)	1445.0/1443.0/	1444.0/1442.0/	1435.3	44.0
	1441.0/1439.0	1441.0/1436.0		
δ(CH)	1400.0/1397.0	1400.0/1396.0	1399.1	9.2
ν(CC), ν(CN)	1355.0	1350.0	1335.9	22.6
δ(CH)	1299.0/1293.0	1297.0/1293.0	1288.2	23.3
	1263.0/1261.0	1262.0/1260.0	1250.4	61.3
δ(NH)	1254.0/1250.0	1251.0/1249.0	1241.6	59.2
ν(CO), δ(CH)	1234.0/1233.0/	1232.0/1231.0/	1230.4	113.6
	1231.0	1228.0		
δ(COH), δ(CH)	1201.0/	1205.0/1202.0/	1191.2	43.6
	1199.01194.0	1200.0/1195.0		
δ(CH)	1161.0/1158.0	1158.0/1155.0	1156.9	19.9
δ(CH)	1147.5/1144.0/	1147.0/1140.0	1139.0	21.1
	1143.0			
ν(CO), ν(CC)	1092.0/1087.0	1089.0/1087.0	1075.3	59.8
ν(CC)	1036.0	1035.5	1035.2	7.1
γ(CH)	n.obs.	n.obs.	977.1	0.0
	n.obs.	n.obs.	951.9	1.7
ν(CN), ν(CC)	960.0/950.0	958.0/950.0	948.0	19.3
δ(ring)	897.0	896.0	884.6	2.0
γ(CH)	840.5	840.0	853.5	0.5
	832.0	834.0	839.9	44.2
γ(CH) all in-phase	767.0/765.0/764.0	764.0/763.0/	761.9	60.8
		761.0		
δ(ring)	756.0/755.0	754.0	753.5	3.5
γ(CH), τ(ring)	754.0/753.0/752.0	753.0/751.0/	746.4	22.2
		750.0		
γ(C=O)	721.0	719.0	717.9	1.0
δ(ring)	666.0	665.0	662.8	4.9
τ(ring)	636.0	n.i.	633.9	0.5
γ(NH)	596.0/593.0/591.0		596.1	59.2
δ(C=O), δ(CO)			595.1	2.2
δ(ring)	534.0		531.4	3.1
τ(ring)	524.0		523.3	0.7
δ(ring)	507.0		489.3	11.7

[a] Wavenumbers in cm^{-1}, calculated intensities in km mol^{-1}.
[b] ν = stretching; δ = in-plane bending; γ = out-of-plane rocking; τ = torsion.
[c] n.obs. = not observed; n.i. = not investigated.
[d] The calculated harmonic wavenumbers were scaled by 0.978 and 0.954 for wavenumbers below and above 3000 cm^{-1}, respectively.

Table 3
Experimental (matrix-isolation) and DFT(B3LYP)/6–311++*G*(3df,3pd) calculated infrared spectra of 2,4-QO and proposed vibrational assignments.

Approximate Description[a]	Experimental		Calculated	
	Argon matrix ν	Xe matrix ν	ν	I^{IR}
ν(NH)	3431.0	3412.0	3426.1	38.2
ν(CH)	3092.0/3068.0/	3089.0/3068.0/	3058.5	7.9
	3059.0/3042.0	3059.0/3048.0/	3047.5	3.0
		3030.0	3037.0	7.3
			3023.2	4.4
$\nu(CH_2)$ as.	n.obs.	n.obs.	2973.8	0.1
$\nu(CH_2)$ s.	2888.0/2886.0	2886.0	2890.8	1.2
ν_1(C=O) s.	1731.0/1723.5	1731.0/1725.0	1737.7	477.6
ν_2(C=O) as.	1705.0	1699.0	1709.2	410.3
ν(CC)	1618.0	1616.0	1609.3	171.6
	1586.0	1590.0/1586.0	1586.5	18.7
	1496.0	1493.0 /1491.0	1491.7	26.8
ν(CC), δ(CH)	1486.0	1483.0	1479.4	161.0
δ(NH), δ(CH)	1420.0/1412.0	1419.0/1409.5	1410.6	9.9
$\delta(CH_2)$	1380.0/1375.0	1377.0/1368.0	1385.0	3.6
ν(CC), ν(CN)	1344.0/1342.0	1342.0/1338.0	1328.0	222.0
ν(CC)	1330.0/1321.0	1320.0/1318.0	1313.8	140.0
wag(CH_2)	1280.5/1274.0	1281.0/1278.0/	1268.6	1.5
		1276.0		
ν(CC), δ(CH)	1268.0/1265.5	1271.0/1268.0	1254.2	31.2
ν(CC), δ(NH)	1241.0/1240.0	1243.0/1240.0/	1234.8	7.4
		1238.0		
ν(CC), δ(CH)	1225.0/1223.0	1225.0/1222.0	1211.6	35.1
twist(CH_2)	1173.0	1177.0	1170.8	2.9
δ(CH)	1163.0	1158.0	1157.9	23.6
δ(CH)	1120.0	1116.0	1115.1	7.4
ν(CC)	1072.0/1064.0	1069.5/1066.0/	1051.0	0.2
		1064.5		
ν(CC)	1028.0	1027.0/1017.5	1022.6	6.1
γ(CH)	n.obs.	n.obs.	989.4	0.1
	975.0	972.0	969.6	0.6
γ(CH_2), γ(C=O) s	927.0	923.0	924.1	8.6
δ(ring)	921.0	918.0	909.9	5.8
δ(ring)	873.0	873.0	863.1	4.0
γ(CH)	n.obs.	n.obs.	858.4	0.3
γ(CH) all in-phase	759.5/758.0	759.0/758.0/757.0	761.1	74.0
δ(ring)	742/746.0	744.0	736.0	12.9
τ(ring)	735.5	732.0	725.6	2.0
δ(ring)	671.0	669.0	662.9	5.7
γ(NH)	642.0	n.i.	646.4	23.3
δ(ring), δ(C=O) as	617.0		613.3	5.6
γ(NH), γ(C=O) as	584.0		590.7	39.4
τ(ring)	529.0		525.8	9.6
δ(ring)	521.0		518.7	1.1
τ(ring), γ(CH_2)	493.0		488.2	11.2

[a] Wavenumbers in cm^{-1}, calculated intensities in km mol^{-1}. [b]ν = stretching; δ = in-plane bending; γ = out-of-plane rocking; τ = torsion; twist = twisting; wag = wagging; s. = symmetric; as. = antisymmetric. [c]n.obs. = not observed; n.i. = not investigated. [d]The calculated harmonic wavenumbers were scaled by 0.978 and 0.954 for wavenumbers below and above 3000 cm^{-1}, respectively.

equilibrium existing prior to deposition, that is an intramolecular process taking place in the gas phase. Indeed, the estimated "equilibrium" population at 423 K of 2,4-QO and *cis*-4HQ2O should be *ca.* 40 and 60 %. In Fig. 3(c), the calculated spectra of the two tautomers were plotted with their intensities not being subjected to any scaling, *i.e.* assuming equal populations (50 %: 50 %). It is clear in the figure that the calculated relative intensities of the bands due to the two species fit rather well those experimentally observed in both matrices.

Below, the discussion of the assignments will only focus on the most intense bands and some of the most characteristic vibrations of the two trapped species. In the high frequency region, *cis*-4HQ2O gives rise to two doublets of bands in both argon and xenon matrices. The first is assigned to the ν(OH) stretching mode and is observed at 3619.0/3617.0 cm^{-1} (Ar) and 3588.0/3579.0 cm^{-1} (Xe) (predicted at 3641.5 cm^{-1}), while the second is observed at 3434.0/3437.5 and 3419.0/3416.0 cm^{-1}, in argon and xenon matrices, respectively, and is ascribed to the ν(NH) stretching mode (predicted at 3432.6 cm^{-1}). The ν(NH) stretching mode of 2,4-QO is predicted at 3426.1 cm^{-1} and is assigned to the shoulder observed at 3412.0 cm^{-1}. The single ν(C=O) stretching vibration of *cis*-4HQ2O is predicted to give rise to an intense band (927.1 km mol^{-1}) at 1697.2 cm^{-1}, and, accordingly, is observed experimentally as intense site-split multiplets at 1697.0/1695.0 (Ar) and 1692.0/1687.0/1683.0/1676.5 (Xe) cm^{-1}. The two carbonyl modes of 2,4-QO are better described as symmetric and antisymmetric combinations of the individual oscillators and are predicted to occur at higher frequencies (symmetric: 1737.7; antisymmetric: 1709.2 cm^{-1}). In good agreement with the theoretical predictions, the bands corresponding to these modes are observed at 1731.0/1723.5 and 1705.0 cm^{-1} in argon, and at 1725.0/1731.0 and 1699.0 cm^{-1} in xenon. According to the calculations,

both the ν(CO) and δ(COH) vibrations contribute significantly to two modes, all of them being intense in infrared (predicted intensities above 43 km mol^{-1}), as expected due to the polarity of the CO and OH bonds. The ν(CO) stretching contributes to the modes predicted at 1230.4 cm^{-1} (mixed with in-plane δ(CH) bending vibrations) and at 1075.3 cm^{-1} (mixed with ν(CC) ring stretching vibrations), while the δ(COH) bending contributes to the modes predicted at 1435.3 and 1191.2 cm^{-1} (in both cases mixed with in-plane δ(CH) bending vibrations). In agreement with the predictions, the corresponding experimental bands are intense and appear as site-split multiplets, centered at values close to those predicted by the calculations (see Table 2).

The vibrations of the amine group present in both *cis*-4HQ2O and 2,4-QO include, besides the ν(NH) stretching mode discussed above, the in-plane δ(NH) bending mode and the out-of-plane γ(NH) rocking vibration, which are also predicted to give rise to intense infrared bands. In *cis*-4HQ2O, these modes are predicted at 1241.6 and 596.1 cm^{-1} with an intensity of 59.2 km mol^{-1} (both modes), and are observed in argon matrix at 1254.0/1250.0 and 596.0/593.0/591.0 cm^{-1}, respectively (in xenon, the first band is observed at 1251.0/1249.0 cm^{-1}, while the region where the second band should be observed was not investigated), in good agreement with the theory. In 2,4-QO, both δ(NH) and γ(NH) vibrations are mixed with vibrations of other groups in two different modes each. The δ(NH) are predicted at 1410.6 and 1234.8 cm^{-1}. These are mixed with in-plane δ(CH) bending vibrations and ν(CC) ring stretching vibrations, respectively. On the other hand, the γ(NH) vibrations appear at 646.4 and 590.7 cm^{-1}. The first is an essentially pure mode, while the second is mixed with the antisymmetric out-of-plane γ(C=O) rocking. The predicted intensities of these four modes are considerably lower than those predicted for the essentially pure δ(NH) and γ(NH) vibrations in *cis*-4HQ2O, being in all cases lower than 40 km mol^{-1} (see Table 3).

Some additional intense modes in the spectra of *cis*-4HQ2O correspond to a ν(CC) ring stretching vibration involving the bonds in the C(3, 4, 5, 6, 7) and C(8, 9, 10) fragments, with adjacent bonds vibrating in opposition of phase (predicted at 1630.8 cm^{-1}, and observed at 1637.0 and 1638.0 cm^{-1} in argon and xenon, respectively) and the all-in-phase out-of-plane γ(CH) mode (predicted at 761.9 cm^{-1}, and observed as site-split features at 767.0/765.0/764.0 and 764.0/763.0/761.0 cm^{-1}, in argon and xenon, respectively). These two modes are also predicted and observed as intense bands in the spectra of 2,4-QO at frequencies similar to those found in *cis*-4HQ2O (calc: 1609.3 and 761.1 cm^{-1}; argon matrix: 1618.0 and 759.5/758.0 cm^{-1}; xenon matrix: 1616.0 and 759.0/758.0/757.0 cm^{-1}).

3.2.2. Results of UV irradiation of the as-deposited argon matrix

The as-deposited argon matrix containing both *cis*-4HQ2O and 2,4-QO was subjected to broadband UV irradiation (λ > 283 nm), as described in Section 3.1. The experimental ultraviolet absorption spectrum of 4HQ2O (in methanol) exhibits two intense bands with maxima at ~314 and ~269 nm [34]. According to the accomplished TD-DFT (B3LYP)/6–311++*G*(3df,3pd) calculations, these bands shall be assigned to the $S_1 \leftarrow S_0$ and $S_5 \leftarrow S_0$ transitions (both of $\pi^* \leftarrow \pi$ type), predicted at 305.3 and 232.9 nm, respectively, and that involve essentially the HOMO → LUMO and HOMO → LUMO+1 // HOMO-1 → LUMO transitions (Table S4). Thus, in the performed excitation (with λ > 283 nm) the bright state corresponds to the S_1 state, involving mostly the HOMO → LUMO transition. For 2,4-QO, the TD-DFT calculations indicate that the bright state in the performed irradiation experiments is mostly S_2 ($\pi\pi^*$), with excitation (323.1 nm) predicted to correspond essentially also to the HOMO → LUMO transition (Table S5).

After *ca.* 9 h of irradiation, ~63% of the initially present species were consumed, as determined by the reduction of intensity of the bands belonging to the reactants. The bands assigned to the two forms decreased in intensity at nearly the same rate, with those assigned to *cis*-4HQ2O experiencing only a marginally faster decay. These results indicate that the global efficiency of the photoprocesses undergone by the two reactant species is essentially identical. Concomitantly with the reduction of the intensity of the bands due to *cis*-4HQ2O and 2,4-QO, new bands emerged in the spectra, testifying the formation of a new species.

In the spectra of the photolyzed matrix, two distinct features with absolute maxima at 2272.0 and 2137.0 cm^{-1} are easily identified as being due to isocyanic acid (HNCO) and carbon monoxide (CO), respectively [47–52]. The last feature shows a multiplet structure, which is a clear indication of the participation of CO molecules in different types of associates. Other characteristic bands of isocyanic acid are observed at 3553.5, 769.0, and 566.5 cm^{-1}. The frequency values for the bands of isocyanic acid observed in the present study somewhat deviate from previously reported values for the isolated molecule of the compound in an argon matrix (3516.8/3505.7, 2259.0, 769.8, 573.7 cm^{-1}) [51], indicating that the photogenerated HNCO molecules are also interacting with other photoproducts produced from the same reactant molecule. Indeed, the cage confinement conditions imposed on a matrix-isolated molecule make it highly improbable for the photoproduced fragments to diffuse away from their original matrix cage. In this case, while cross reactions involving fragments produced from different molecules are generally inaccessible, the different species formed in the same cage (from the same original molecule) most of the time interact with each other.

Other bands of the photoproducts were observed in the photolyzed matrix besides those ascribable to HNCO and CO. Among possible products that can result from the reactant molecules upon extrusion of CO, HNCO or CO + HNCO, it was possible to identify in the spectra of the photolyzed matrix two sets of bands that fit well the calculated infrared spectra of 1,3-dihydro-2*H*-indol-2-one (DHI) and cyclohepta-1,2,4,6-tetraene (CHT). The first molecule results from extrusion of CO from the reactant species, while the second results from extrusion of both CO and HNCO. Additionally, a third set of bands could be ascribed to *cis*-2HQ4O(3*H*), which can be obtained directly from 2,4-QO by [1,3] H-atom transfer from the amine group of this molecule to its vicinal carbonyl group. Fig. 4 summarizes the photoreactions proposed to take place upon the performed UV irradiations. It is worth noticing that no evidence of the higher-energy *trans* conformer of 2HQ4O(3*H*) was found in the spectra of the matrix after UV irradiation. This strongly suggests that the formation of *cis*-2HQ4O(3*H*) takes place *via* a concerted mechanism, considering the favorable geometric orientation of the H-donor and acceptor groups in the reactant species leading to formation of this conformer. In any case, if the *trans* conformer was formed one would expect its prompt decay, by quantum mechanical tunneling, to the more stable *cis* conformer, considering that the *trans*→*cis* barrier is only of *ca.* 20 kJ mol^{-1}; see Section 2.2. On the other hand, the mechanism of formation of CTH cannot be extracted from the experimental data. However, it appears reasonable to state that, together with the CO and HNCO leaving fragments, carbene (:CH_2) and benzyne (C_6H_4) were also generated. These species promptly reacted *via* a rapid ring-expansion reaction, by insertion of the carbene into a CC bond, thus leading to the formation of CHT. Alternatively, it is possible that bicycle [4.1.0]hepta-1,3,5-triene was initially formed following the extrusion of CO and HNCO, subsequently undergoing fast opening of its 3-membered ring, generating CHT.

The assignment of the bands to the different photoproducts is given in Table 4, where the observed frequencies are compared with the calculated values and, where available, with previously reported data. Band marks for CHT, DHI, and *cis*-2HQ4O(3*H*) are observed, correspondingly, at 1842.5 and 775.0 cm^{-1} (calculated at 1842.1 and 788.8 cm^{-1} and observed previously experimentally at 1824.0/1816.0 and 771.0 cm^{-1} [53]), 3485.0 and 1746.0/1740.5 (calculated: 1764.7 cm^{-1}), and 3573.5, 1669.5, and 1137.5/1133.0 cm^{-1} (calculated: 3567.2, 1665.4, and 1144.0 cm^{-1}). The spectroscopic data showing the results of the UV irradiation (obtained after 530 min. of irradiation) are shown in Fig. 5, where the experimental results are compared with the relevant calculated data. Fig. 6 displays the evolution of the relative amounts of

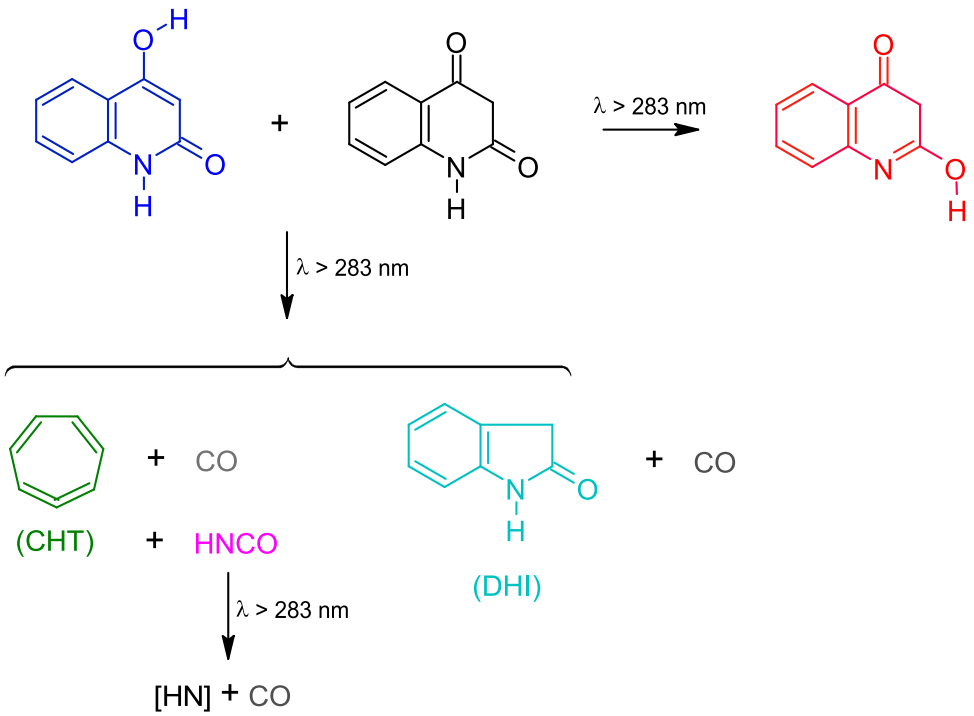

Fig. 4. Proposed photochemical reactions taking place upon UV (λ = 283 nm) photolysis of *cis*-4HQ2O/2,4-QO in an argon matrix.

various species in the matrix over time, as determined by the changes in the intensities of selected characteristic bands of each species with irradiation. The chosen bands correspond to intense mark-bands of each compound that appear well-separated from other bands, thus allowing to minimize the error in the intensity measurements. The wavenumber ranges used for band area integrations are indicated in the caption of Fig. 6.

To calculate the relative amounts from the band intensities, the following procedure was used, which took into account the mechanism shown in Fig. 4 and assumed that the two reactants (*cis*-4HQ2O and 2,4-QO) were reacting at the same rate (as suggested by the relative changes of their individual spectra along the irradiation, as it has already been mentioned above). At each point, the sum of the amounts of CHT, DHI, and *cis*-2HQ4O(3*H*) must equal the total amount of the consumed reactants, so that the percent of reduction of intensity of the mark-band of the two reactants used in the performed calculations, weighted by the average of the corresponding calculated band intensities, must equal the sum of the band intensities of CHT, DHI, and *cis*-2HQ4O(3*H*) weighted by their calculated intensities. After 530 min of UV irradiation, the amount of reactants decreased by ~63%, with CHT comprising 57%, DHI *ca.* 1%, and *cis*-2HQ4O(3*H*) 5%. These numbers demonstrate that the pathway leading to extrusion from the reactant species of both CO and HNCO strongly dominates over that leading to extrusion of CO only.

The amounts of CO and HNCO are correlated because HNCO can be expected to be photolyzed to CO, along with HN. However, the experimental observation of HN is challenging. Its unique IR band, observed in gas phase at 3125.0 cm^{-1} [54], lies in a congested spectral range where the CH stretching modes of the reactants and remaining products are also observed. Normalization of the HNCO band intensity by its DFT calculated intensity (757.7 km mol^{-1}), compared to that expected if the photo-decomposition of HNCO was not taking place (case where the amounts of HNCO and CHT should be equal), revealed that about half of the HNCO molecules initially formed underwent photo-decomposition to CO and HN. After 530 min of UV irradiation, the amount of HNCO in the matrix corresponds to ~29% (taking the initial amount of reactants as reference). The amount of CO can then be calculated as being equal to 1.5 times that of CHT plus that of DHI (*ca.* 87% of the initial amount of the reactants). However, these calculations do not fit the experimental data when the intensity of the CO band, normalized by the corresponding DFT predicted IR intensity for the monomer (79.8 km mol^{-1}), is directly used to estimate the amount of CO. In this case, the amount of CO is estimated to be considerably larger than the expected value presented above. To fit the quantity of CO prediction, a correction factor of about 2 must be applied to the DFT calculated IR intensity of the CO band. The need for such correction is in line with the involvement of the CO molecules in different associates with other species present in the matrix-cage after photolysis (including in the form of CO dimeric structures), which has already been pointed out based on the observed complex profile of the CO band.

It is interesting to note that in the spectra of the photolyzed matrix, no evidence was found of the presence of the molecules that could result from exclusive HNCO extrusion, either directly from 2,4-QO or *cis*-4HQ2O, specifically benzocyclobutanone or its enol tautomer, the same applying to 2,4-QOH and 2HQ4O(1*H*) tautomeric forms of 4HQ2O, which were also not identified in the photolyzed matrix.

4. Conclusion

In the present work, 4-hydroxyquinolin-2(1*H*)-one was investigated by infrared spectroscopy in argon and xenon matrices and by theoretical calculations carried out at the DFT(B3LYP) level of theory using the 6–311++*G*(3df,3pd) basis set. The five lowest tautomeric structures predicted by the calculations were characterized structurally and conformationally, and their relative energies and most significant structural differences were rationalized in terms of the distinct intramolecular interactions they exhibit.

Two tautomeric forms (*cis*-4HQ2O and 2,4-QO), whose identity could be established with help of the theoretical data, were found to be present in the as-deposited cryogenic matrices (argon, xenon). Among the different tautomeric forms of the studied compound, these two forms correspond to those having the lowest energies (with 2,4-QO being only 4.8 kJ mol^{-1} higher in energy than the most stable *cis*-4HQ2O form when the zero-point correction is considered; the standard free Gibbs energy difference between these forms at 298.15 K calculated at the DFT

Table 4
Assignment of the bands due to the products of the photochemical reactions taking place upon UV (λ = 283 nm) photolysis of *cis*-4HQ2O/2,4-QO in an argon matrix.[a]

Approximate Description[b]	Exp. Ar matrix	Calculated[c]						Exp. Ar matrix [49]	Exp. Ar matrix [51]
		cis-2HQ4O(3*H*)		CHT[d]		DHI		CO	HNCO
	ν	ν	I^{IR}	ν	I^{IR}	ν	I^{IR}	ν	ν
ν(OH)	3573.5	3567.2	74.2						
ν(NH)	3535.5								3516.8/ 3505.7
ν(NH)	3485.0					3471.4	47.8		
ν(NCO) as	2272.0/2265.0/ 2260.5								2259.0
ν(CO)	2157.0/2155.5/ 2152.0/2150.0/ 2143.0/2141.0/ 2138.0/2137.0/ 2129.5/2127.0/ 2123.5							2140.1/ 2138.5/ 2136.7	
ν(C=C=C) as	1842.5			1842.1	15.3				
ν(C=O)	1746.0/1740.5					1764.7	661.3		
ν(C=O)	1714.0	1712.9	303.2						
ν(C=N)	1669.5	1665.4	438.0						
ν(C=C) ph	1637.5					1622.0	72.7		
ν(C=C) ph	1625.0	1601.4	134.6						
ν(C=C) as	1590.0			1578.2	2.7				
ν(C=C) ph	1571.0	1564.3	26.4						
δ(CH), ν(C=C) ph	1477.0	1466.5	75.6			1469.5	68.3		
δ(COH), wag(CH_2), ν(CC)	1406.5	1400.8	60.1						
δ(CH) s	1391.5			1380.6	14.4				
δ(CH_2) // δ(NH) (DHI)	1384.5	1375.1	76.6			1388.4	38.3		
ν(C=C=C) s	1360.0			1355.3	14.6				
ν(C=C) pH, δ(COH)	1311.0	1303.7	12.7						
δ(CH), wag(CH_2), δ(COH)	1304.5	1301.0	21.9						
δ(CH) s (allene)	1287.0			1280.1	3.8				
ν(CCC) as, δ(CH)	1275.0	1278.2	98.8						
ν(CN), wag(CH_2)	1256.0					1250.4	36.3		
ν(CN), wag(CH_2), ν(C–—O)	1245.0	1237.2	36.3						
ν(NC), δ(NH), wag(CH_2)	1208.0					1209.3	47.2		
wag(CH_2), ν(CN)	1185.0					1192.9	62.8		
δ(CH) as	1181.0			1189.9	1.9				
δ(CH) ph	1147.0	1158.5	58.3			1157.3	21.9		
						1154.2	30.1		
δ(COH), ν(C—O)	1137.5/1133.0	1144.0	251.0						
δ(CH) as (allene)	1099.0			1101.1	3.6				
ν(CC) ph	1074.5					1090.9	25.5		
ν(CC) ph	1027.5	1019.7	6.3			1020.1	6.4		
γ(CH) as	979.0			978.1	4.0				
γ(CH) as // γ(CH_2) (DHI)	953.5			957.9	2.1	953.5	4.0		
γ(CH) s (allene)	775.0			788.8	63.3				
δ(HNC)	769.0								769.8
γ(CH) s	761.0/756.0	771.0	59.9						
γ(CH) s ph	748.0/740.0					746.6	57.5		
δ(ring) pH, δ(C–C=N)	717.0	729.9	13.8						
τ(ring) ph	707.0					703.9	7.3		
δ(C=C=C)	697.0			689.6	23.5				
γ(CH) s	678.5			681.5	79.4				
δ(ring) ph, δ(CNC)	662.0					668.8	13.5		
δ(ring) ph	661.0	655.8	12.3						
γ(OH)	630.0	629.6	25.5						
δ(NCO)	566.5								573.7
γ(NH)	547.5					538.9	43.4		
δ(CO)	530.0					526.5	13.5		

[a] Wavenumbers in cm^{-1}, calculated intensities in km mol^{-1}.

[b] ν = stretching; δ = in-plane bending; γ = out-of-plane rocking; τ = torsion; wag = wagging; s. = symmetric; as. = antisymmetric; ph = phenyl ring; when a band is assigned to two species and the approximate descriptions are different, these are separated by // with the first description of the mode applying to the species indicated in the column most at the left and the second to the species indicated in the column most at the right.

[c] The calculated harmonic wavenumbers were scaled by 0.978 and 0.954 for wavenumbers below and above 3000 cm^{-1}, respectively.

[d] In a previous argon matrix study [53], mark bands of CHT have been observed at 1824.0/1816.0 (ν(C=C=C) as), 1380.0 (δ(CH) s), 1270.0 (δ(CH) s (allene)), 771.0 (γ(CH) s (allene)), 690.0 (δ(C=C=C)), and 679.0 (γ(CH) s), in good correspondence with those observed in the present study.

(B3LYP)/6–311++*G*(3df,3pd) level of theory is even smaller, being only 1.9 kJ mol^{-1}). A rationale was presented for the observation of the 2,4-QO tautomer in the as-deposited matrices, which considers occurrence of tautomerization upon sublimation, presumably taking place in the solid-gas interface, as found before for other tautomeric systems, in particular when the tautomeric forms involved have similar energies. The absence of the *trans*-4HQ2O conformer in the as-deposited matrices, which can be expected to be significantly populated in the gas phase equilibrium prior to deposition of the matrices, was explained by its rapid conversion to the more stable *cis*-4HQ2O form during matrix

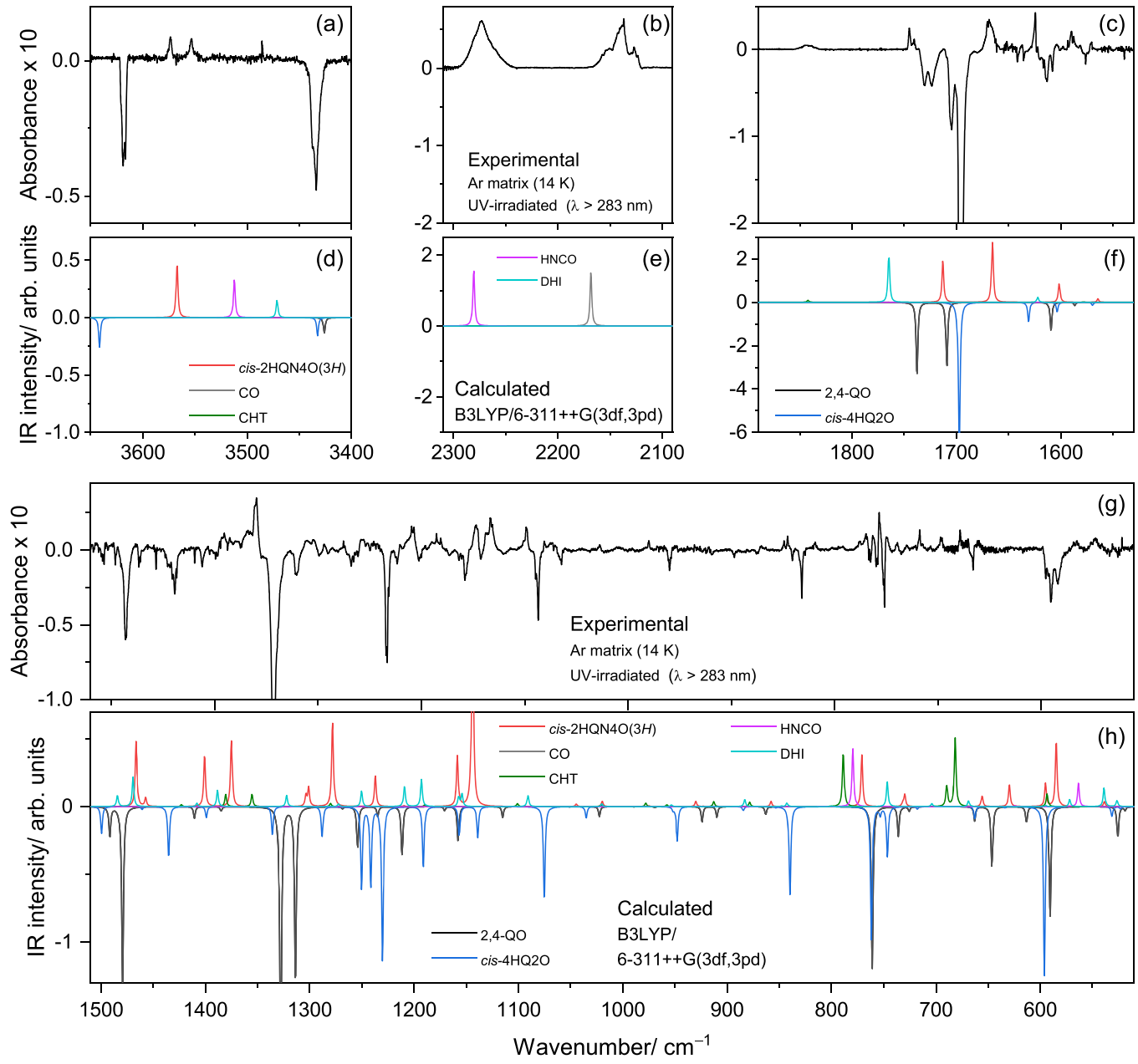

Fig. 5. Experimental difference FTIR spectrum of 4HQ2O isolated in Ar matrices after UV irradiation at λ > 283 nm (after 530 min) *minus* the spectrum of the as-deposited 4HQ2O (a–c, g) compared with the simulated difference infrared spectrum of the harmonic frequencies of the most stable tautomer *cis*-4HQ2O and 2,4-QO tautomer *minus* the sum of *cis*-2HQ4O(3*H*) and *trans*-2HQ4O(3*H*) calculated at the DFT(B3LYP)/6–311++*G*(3df,3pd) level of theory (d–f, h). The calculated harmonic frequencies were scaled by 0.978 and 0.954 for frequencies below and above 3000 cm^{-1}, respectively. Some of the most intense bands of have been truncated for clarity.

deposition *via* the tunnelling mechanism (by internal rotation around the C–OH bond, through the low *trans*-4HQ2O → *cis*-4HQ2O isomerization energy barrier of 12.8 kJ mol^{-1}). A comprehensive assignment of the IR spectra of both *cis*-4HQ2O and 2,4-QO isolated in Ar and Xe matrices was presented.

The photochemistry of the studied compound in solid argon upon *in situ* ultraviolet irradiation (λ > 283 nm; bright state: S_1) of the as-deposited matrix was investigated. Following irradiation, the two forms initially present in the matrix, *cis*-4HQ2O and 2,4-QO, were found to react at nearly the same rate, generating an additional tautomeric form, *cis*-2HQ4O(3*H*), together with products of fragmentation of the heterocyclic ring of the molecules, specifically isocyanic acid, carbon monoxide, 1,3-dihydro-2*H*-indol-2-one, and cyclohepta-1,2,4,6-tetraene. The relative amounts of the different species present in the irradiated matrix were estimated from the observed intensity changes of their selected band-marks along the irradiation time. It was shown that the pathway leading to extrusion from the reactant species of both CO and HNCO strongly dominates over that leading to extrusion of CO only. Furthermore, no evidence was found in the spectra of the photolyzed matrix of any putative photoproduct resulting solely from the extrusion of HNCO. The kinetic studies also revealed that, under the used experimental conditions, approximately half of the formed HNCO molecules undergo a subsequent reaction to CO (plus non-observed NH). In addition, both the spectroscopic and kinetic data revealed that CO molecules form different associates with other species present in the matrix-cage where they are formed (including CO dimeric structures).

Overall, the present study contributes to expanding the available knowledge on the structure, tautomerism, and photochemistry of 4-

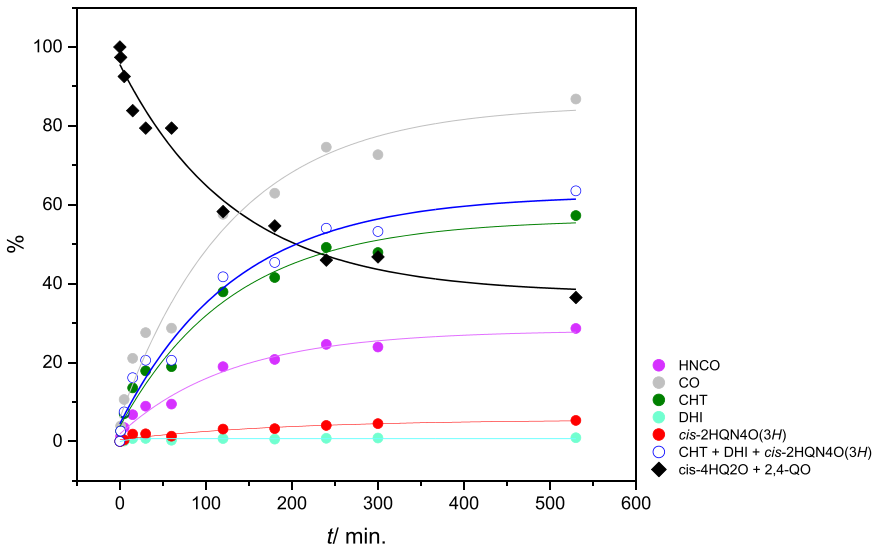

Fig. 6. Evolution of the relative amounts of the different species present in the matrix with the time of irradiation, obtained from the changes in the integrated intensities of selected characteristic bands of each species. Bands/region used: *cis*-4HQ2O/2,4-QO: 3445–3425 cm^{-1}; *cis*-2HQ4O(3*H*): 1143–1120 cm^{-1}; HNCO: 2285–2243 cm^{-1}; CO: 2177–2120 cm^{-1}; DHI: 1748–1738 cm^{-1}; CHT: 1855–1825 cm^{-1}. See text for details.

hydroxyquinolin-2(1*H*)-ones.

CRediT authorship contribution statement

A. Secrieru: Writing – review & editing, Investigation, Formal analysis, Conceptualization. **S. Lopes:** Writing – review & editing, Writing – original draft, Investigation, Formal analysis. **T. Nikitin:** Writing – review & editing, Investigation. **Maria L.S. Cristiano:** Writing – review & editing, Supervision, Funding acquisition, Formal analysis. **R. Fausto:** Writing – review & editing, Supervision, Funding acquisition, Formal analysis.

Declaration of competing interest

The authors declare that they have no known competing financial interests or personal relationships that could have appeared to influence the work reported in this paper.

Data availability

Data will be made available on request.

Acknowledgements

This work has run within the research project PTDC/QUI-QFI/1880/2020. The CQC-IMS is supported by the Fundação para a Ciência e a Tecnologia (FCT), through projects UI0313B/QUI/2020 (DOI: 10.54499/UIDB/00313/2020), UI0313P/QUI/2020 (DOI: 10.54499/UIDP/00313/2020), and LA/P/0056/2020. Fundação para a Ciência e a Tecnologia (FCT) is also acknowledged for projects UIDB/04326/2020 (DOI:10.54499/UIDB/04326/2020), UIDP/04326/2020 (DOI:10.54499/UIDP/04326/2020), LA/P/0101/2020 (DOI:10.54499/LA/P/0101/2020, CCMAR-CIMAR), and grant SFRH/BD/140249/2018 (AS). The authors also acknowledge the Laboratory for Advanced Computing at University of Coimbra (https://www.uc.pt/lca) for providing computing resources and LaserLab Coimbra for experimental facilities.

Supplementary materials

Supplementary material associated with this article can be found, in the online version, at doi:10.1016/j.molstruc.2024.138412.

References

[1] S. Kumar, S. Bawa, H. Gupta, Biological activities of quinoline derivatives, Mini-Rev. Med. Chem. 9 (2010) 1648–1654, https://doi.org/10.2174/138955709791012247.
[2] F. O'Donnell, T.J.P. Smyth, V.N. Ramachandran, W.F. Smyth, A study of the antimicrobial activity of selected synthetic and naturally occurring quinolines, Int. J. Antimicrob. Agents 35 (2010) 30–38, https://doi.org/10.1016/j.ijantimicag.2009.06.031.
[3] W.P. Hong, I. Shin, H.N. Lim, Recent advances in one-pot modular synthesis of 2-quinolones, Molecules (2020), https://doi.org/10.3390/MOLECULES25225450.
[4] A.A. Aly, M. Ramadan, G.E.D.A. Abuo-Rahma, Y.A.M.M. Elshaier, M.A. I. Elbastawesy, A.B. Brown, S. Bräse, Quinolones as prospective drugs: their syntheses and biological applications, Adv. Heterocycl. Chem. 135 (2021) 147–196, https://doi.org/10.1016/bs.aihch.2020.08.001.
[5] R. Watpade, A. Bholay, R. Toche, Synthesis of new pyrano-fused quinolines as antibacterial and antimicrobial agents, J. Heterocycl. Chem. 54 (2017) 3434–3439, https://doi.org/10.1002/jhet.2966.
[6] H.M. Hassanin, S.M. El-Edfawy, Novel heterocyclic dertvatives of 2-quinolinone associated with antibacterial and antitumor potencies, Heterocycles 85 (2012) 2421–2436, https://doi.org/10.3987/COM-12-12523.
[7] M.S. Katagi, G.S. Bolakatti, A.M. Badiger, D. Satyanarayana, S.N. Mamledesai, M. L. Sujatha, Synthesis, spectral characterization and antimicrobial activity of substituted thiazolyl derivatives of 2-quinolones, Drug Res. 63 (2013) 53–59, https://doi.org/10.1055/s-0032-1331711 (Stuttg).
[8] A.A. Boteva, O.P. Krasnykh, The methods of synthesis, modification, and biological activity of 4-quinolones (review), Chem. Heterocycl. Compd. 45 (2009) 757–785, https://doi.org/10.1007/s10593-009-0360-1.
[9] N. Talaat, M. Abass, H.M. Hassanin, D. Abdel-Kader, Synthesis and anticancer activity of oxazolo and oxazinoquinolinone derivatives, Synth. Commun. 52 (2022) 1756–1767, https://doi.org/10.1080/00397911.2022.2112962.
[10] M. Abass, B.B. Mostafa, Synthesis and evaluation of molluscicidal and larvicidal activities of some novel enaminones derived from 4-hydroxyquinolinones: part IX, Bioorg. Med. Chem. 13 (2005) 6133–6144, https://doi.org/10.1016/j.bmc.2005.06.038.
[11] P.C. Appelbaum, P.A. Hunter, The fluoroquinolone antibacterials: past, present and future perspectives, Int. J. Antimicrob. Agents 16 (2000) 5–15, https://doi.org/10.1016/S0924-8579(00)00192-8.
[12] J. Jampilek, R. Musiol, M. Pesko, K. Kralova, M. Vejsova, J. Carroll, A. Coffey, J. Finster, D. Tabak, H. Niedbala, V. Kozik, J. Polanski, J. Csollei, J. Dohnal, Ring-substituted 4-hydroxy-1h-quinolin-2-ones: preparation and biological activity, Molecules 14 (2009) 1145–1159, https://doi.org/10.3390/molecules14031145.
[13] T. Khamkhenshorngphanuch, K. Kulkraisri, A. Janjamratsaeng, N. Plabutong, A. Thammahong, K. Manadee, S.Na Pombejra, T. Khotavivattana, Synthesis and antimicrobial activity of novel 4-Hydroxy-2-quinolone analogs, Molecules 25 (2020) 1–12, https://doi.org/10.3390/molecules25133059.
[14] G.A. Borges e Soares, T. Bhattacharya, S. Mamledesai, Z. Ai, A.M. Hasan, S. Cavalu, Identification of linomide derivatives as potential anticancer therapeutics using molecular docking studies, Front. Pharmacol. 13 (2022) 1–10, https://doi.org/10.3389/fphar.2022.892914.

[15] M.B. de Macedo, R. Kimmel, D. Urankar, M. Gazvoda, A. Peixoto, F. Cools, E. Torfs, L. Verschaeve, E.S. Lima, A. Lyčka, D. Milićević, A. Klásek, P. Cos, S. Kafka, J. Košmrlj, D. Cappoen, Design, synthesis and antitubercular potency of 4-hydroxyquinolin-2(1H)-ones, Eur. J. Med. Chem. 138 (2017) 491–500, https://doi.org/10.1016/j.ejmech.2017.06.061.

[16] B.S. Kirkiacharian, E. De Clercq, R. Kurkjian, C. Pannecouque, New synthesis and anti-HIV and antiviral properties of 3-arylsulfonyl derivatives of 4-ydroxycoumarin and 4-hydroxyquinolone, Pharm. Chem. J. 42 (2008) 265–270, https://doi.org/10.1007/s11094-008-0103-0.

[17] E.O.M. Rufchahi, A.G. Gilani, Synthesis, characterization and spectroscopic properties of some new azo disperse dyes derived from 4-hydroxybenzo[h]quinolin-2-(1H)-one as a new synthesized enol type coupling component, Dyes Pigments 95 (2012) 632–638, https://doi.org/10.1016/j.dyepig.2012.06.008.

[18] S. Heeb, M.P. Fletcher, S.R. Chhabra, S.P. Diggle, P. Williams, M. Cámara, Quinolones: from antibiotics to autoinducers, FEMS Microbiol. Rev. 35 (2011) 247–274, https://doi.org/10.1111/j.1574-6976.2010.00247.x.

[19] G.S. Bisacchi, Origins of the quinolone class of antibacterials: an expanded "discovery story, J. Med. Chem. 58 (2015) 4874–4882, https://doi.org/10.1021/jm501881c.

[20] J.C. Jung, Y.J. Jung, O.S. Park, Synthesis of 4-Hydroxyquinolin-2(1H)-one analogues and 2-substituted quinolone derivatives, J. Heterocycl. Chem. 38 (2001) 61–67, https://doi.org/10.1002/jhet.5570380109.

[21] K. Arya, M. Agarwal, Microwave prompted multigram synthesis, structural determination, and photo-antiproliferative activity of fluorinated 4-hydroxyquinolinones, Bioorg. Med. Chem. Lett. 17 (2007) 86–93, https://doi.org/10.1016/j.bmcl.2006.09.082.

[22] M. Rowley, J.J. Kulagowski, A.P. Watt, D. Rathbone, G.I. Stevenson, R.W. Carling, R. Baker, G.R. Marshall, J.A. Kemp, A.C. Foster, S. Grimwood, R. Hargreaves, C. Hurley, K.L. Saywell, M.D. Tricklebank, P.D. Leeson, Effect of plasma protein binding-on *in vivo* activity and brain penetration of glycine/NMDA receptor antagonists, J. Med. Chem. 40 (1997) 4053–4068, https://doi.org/10.1021/jm970417o.

[23] M.J. Frisch, G.W. Trucks, H.B. Schlegel, G.E. Scuseria, M.a. Robb, J.R. Cheeseman, G. Scalmani, V. Barone, G.a. Petersson, H. Nakatsuji, X. Li, M. Caricato, a. V. Marenich, J. Bloino, B.G. Janesko, R. Gomperts, B. Mennucci, H.P. Hratchian, J. V. Ortiz, A.F. Izmaylov, J.L. Sonnenberg, Williams, F. Ding, F. Lipparini, F. Egidi, J. Goings, B. Peng, A. Petrone, T. Henderson, D. Ranasinghe, V.G. Zakrzewski, J. Gao, N. Rega, G. Zheng, W. Liang, M. Hada, M. Ehara, K. Toyota, R. Fukuda, J. Hasegawa, M. Ishida, T. Nakajima, Y. Honda, O. Kitao, H. Nakai, T. Vreven, K. Throssell, J.A. Montgomery Jr., J.E. Peralta, F. Ogliaro, M.J. Bearpark, J. J. Heyd, E.N. Brothers, K.N. Kudin, V.N. Staroverov, T.A. Keith, R. Kobayashi, J. Normand, K. Raghavachari, A.P. Rendell, J.C. Burant, S.S. Iyengar, J. Tomasi, M. Cossi, J.M. Millam, M. Klene, C. Adamo, R. Cammi, J.W. Ochterski, R.L. Martin, K. Morokuma, O. Farkas, J.B. Foresman, D.J. Fox, Gaussian 16, Revision B.01, Gaussian, Inc., Wallinfort CT, 2016.

[24] S.H. Vosko, L. Wilk, M. Nusair, Accurate spin-dependent electron liquid correlation energies for local spin density calculations: a critical analysis, Can. J. Phys. 58 (1980) 1200–1211, https://doi.org/10.1139/p80-159.

[25] A.D. Becke, Density-functional exchange-energy approximation with correct asymptotic behavior, Phys. Rev. A 38 (1988) 3098–3100, https://doi.org/10.1103/PhysRevA.38.3098.

[26] C. Lee, W. Yang, R.G. Parr, Development of the Colle-Salvetti correlation-energy formula into a functional of the electron density, Phys. Rev. B 37 (1988) 785–789, https://doi.org/10.1103/PhysRevB.37.785.

[27] T. Clark, J. Chandrasekhar, G.W. Spitznagel, P.V.R. Schleyer, Efficient diffuse function-augmented basis sets for anion calculations. III. The 3-21+G basis set for first-row elements, Li–F, J. Comput. Chem. 4 (1983) 294–301, https://doi.org/10.1002/jcc.540040303.

[28] M.J. Frisch, J.A. Pople, J.S. Binkley, Self-consistent molecular orbital methods 25. Supplementary functions for Gaussian basis sets, J. Chem. Phys. 80 (1984) 3265–3269, https://doi.org/10.1063/1.447079.

[29] R. Krishnan, J.S. Binkley, R. Seeger, J.A. Pople, Self-consistent molecular orbital methods. XX. A basis set for correlated wave functions, J. Chem. Phys. 72 (1980) 650–654, https://doi.org/10.1063/1.438955.

[30] C. Peng, H.B. Schlegel, Combining synchronous transit and quasi-newton methods to find transition states, Isr. J. Chem. 33 (1993) 449–454, https://doi.org/10.1002/ijch.199300051.

[31] Chemcraft – graphical software for visualization of quantum chemistry computations, (2021).

[32] C. Adamo, D. Jacquemin, The calculations of excited-state properties with time-dependent density functional theory, Chem. Soc. Rev. 42 (2013) 845–856, https://doi.org/10.1039/c2cs35394f.

[33] A.D. Laurent, C. Adamo, D. Jacquemin, Dye chemistry with time-dependent density functional theory, Phys. Chem. Chem. Phys. 16 (2014) 14334–14356, https://doi.org/10.1039/c3cp55336a.

[34] N. Priya, A. Gupta, K. Chand, P. Singh, A. Kathuria, H.G. Raj, V.S. Parmar, S. K. Sharma, Characterization of 4-methyl-2-oxo-1,2-dihydroquinolin-6-yl acetate as an effective antiplatelet agent, Bioorg. Med. Chem. 18 (2010) 4085–4094, https://doi.org/10.1016/j.bmc.2010.04.011.

[35] S.L. Zhang, Z.S. Huang, Y.M. Li, A.S.C. Chan, L.Q. Gu, Synthesis of zwitterionic 4-hydroxy-2(1H)-quinolinone derivatives, Tetrahedron 64 (2008) 4403–4407, https://doi.org/10.1016/j.tet.2008.02.052.

[36] G.M. Coppola, A.D. Kahle, M.J. Shapiro, 13 C NMR investigation of some hetero-ring substituted 2- and 4-quinolone systems, Org. Magn. Reson. 17 (1981) 242–245, https://doi.org/10.1002/mrc.1270170404.

[37] E. Hebanowska, A. Tempczyk, L. Łobocki, J. Szafranek, A. Szafranek, Z. H. Urbanek, Gas phase prototropic equilibrium studies of 2,4-dihydroxyquinoline by cndo/2 calculations, mass spectrometry and derivatization, J. Mol. Struct. 147 (1986) 351–361, https://doi.org/10.1016/0022-2860(86)80389-1.

[38] J. Luis García Ruano, J.H. Rodriguez, C. Pedregal, Synthesis and Tautomerism of 2,4-Dihydroxyquinolines, Heterocycles 32 (1991) 2151, https://doi.org/10.3987/COM-91-5823.

[39] C.A. Coulson, Valence, 2nd ed., Oxford University Press, 1961. https://books.google.pt/books?id=wD23AAAAIAAJ.

[40] R. Fausto, Bonding in carbonyl and thiocarbonyl compounds: an ab initio charge density study of H2C=X and HC(=X)YH (X,Y = O or S), J. Mol. Struct. THEOCHEM 315 (1994) 123–136, https://doi.org/10.1016/0166-1280(94)03787-L.

[41] A. Chatterjee, S.J. Cutler, I.A. Khan, J.S. Williamson, Efficient synthesis of 4-oxo-4,5-dihydrothieno[3,2- c c]quinoline-2-carboxylic acid derivatives from aniline, Mol. Divers. 18 (2014) 51–59, https://doi.org/10.1007/s11030-013-9476-4.

[42] M. Sechi, U. Azzena, M.P. Delussu, R. Dallocchio, A. Dessì, A. Cosseddu, N. Pala, N. Neamati, Design and synthesis of bis-amide and hydrazide-containing derivatives of malonic acid as potential HIV-1 integrase inhibitors, Molecules 13 (2008) 2442–2461, https://doi.org/10.3390/molecules13102442.

[43] R. Fausto, G.O. Ildiz, C.M. Nunes, IR-induced and tunneling reactions in cryogenic matrices: the (incomplete) story of a successful endeavor, Chem. Soc. Rev. 51 (2022) 2853–2872, https://doi.org/10.1039/D1CS01026C.

[44] A.J. Lopes Jesus, C.M. Nunes, I. Reva, S.M.V. Pinto, R. Fausto, Effects of entangled IR radiation and tunneling on the conformational interconversion of 2-cyanophenol, J. Phys. Chem. A 123 (2019) 4396–4405, https://doi.org/10.1021/acs.jpca.9b01382.

[45] A.J. Lopes Jesus, J.R. de Lucena Júnior, R. Fausto, I. Reva, Infrared spectra and phototransformations of meta-fluorophenol isolated in argon and nitrogen matrices, Molecules 27 (2022) 8248, https://doi.org/10.3390/molecules27238248.

[46] L. Lapinski, I. Reva, M.J. Nowak, R. Fausto, Five isomers of monomeric cytosine and their interconversions induced by tunable UV laser light, Phys. Chem. Chem. Phys. 13 (2011) 9676, https://doi.org/10.1039/c0cp02812f.

[47] H. Dubost, Infrared absorption spectra of carbon monoxide in rare gas matrices, Chem. Phys. 12 (1976) 139–151, https://doi.org/10.1016/0301-0104(76)87051-6.

[48] H. Abe, H. Takeo, K.M.T. Yamada, Infrared spectroscopy of CO trapped in an argon matrix revisited, Chem. Phys. Lett. 311 (1999) 153–158, https://doi.org/10.1016/S0009-2614(99)00847-7.

[49] H. Abe, K.M.T. Yamada, Infrared spectra of carbon monoxide in Kr and Xe matrices: shifts of the vibrational line positions, Struct. Chem. 14 (2003) 211–215, https://doi.org/10.1023/A:1022198717855.

[50] B.A. Nogueira, G.O. Ildiz, J. Canotilho, M.E.S. Eusébio, R. Fausto, Molecular structure, infrared spectra, photochemistry, and thermal properties of 1-methylhydantoin, J. Phys. Chem. A 118 (2014) 5994–6008, https://doi.org/10.1021/jp505335c.

[51] J.H. Teles, G. Maier, B. Andes Hess, L.J. Schaad, M. Winnewisser, B. P. Winnewisser, The CHNO isomers, Chem. Ber. 122 (1989) 753–766, https://doi.org/10.1002/cber.19891220425.

[52] S. Lopes, T. Nikitin, R. Fausto, Photochemical study and vibrational spectra of propiolamide isolated in low-temperature Ar, Xe, and N2 matrices, J. Photochem. Photobiol. A Chem. 438 (2023) 114487, https://doi.org/10.1016/j.jphotochem.2022.114487.

[53] R.J. McMahon, C.J. Abelt, O.L. Chapman, J.W. Johnson, C.L. Kreil, J.P. LeRoux, A. M. Mooring, P.R. West, 1,2,4,6-cycloheptatetraene: the key intermediate in arylcarbene interconversions and related C7H6 rearrangements, J. Am. Chem. Soc. 109 (1987) 2456–2469, https://doi.org/10.1021/ja00242a034.

[54] J.Y.P. Mui, R.A. Back, The photolysis of isocyanic acid vapor, Can. J. Chem. 41 (1963) 826–833, https://doi.org/10.1139/v63-119.